Nanoscale

PAPER

View Article Online
View Journal | View Issue

Cite this: *Nanoscale*, 2016, **8**, 13669

Fluorescence and visual detection of fluoride ions using a photoluminescent graphene oxide paper sensor†

Xiaochun Chen,[a] Shaoming Yu,*[a] Liang Yang,[b] Jianping Wang[b] and Changlong Jiang*[b,c,d]

The instant and on-site detection of trace aqueous fluoride ions is still a challenge for environmental monitoring and protection. This work demonstrates a new analytical method and its utility of a paper sensor for visual detection of F^- on the basis of the fluorescence resonance energy transfer (FRET) between photoluminescent graphene oxide (GO) and silver nanoparticles (AgNPs) through the formation of cyclic esters between phenylborinic acid and diol. The fluorescence of GO was quenched by the AgNPs, and trace F^- can recover the fluorescence of the quenched photoluminescent GO. The increase in fluorescence intensity is proportional to the concentration of F^- in the range of 0.05–0.55 nM, along with a limit of detection (LOD) as low as 9.07 pM. Following the sensing mechanism, a paper-based sensor for the visual detection of aqueous F^- has been successfully developed. The paper sensor showed high sensitivity for aqueous F^-, and the LOD could reach as low as 0.1 μM as observed by the naked eye. The very simple and effective strategy reported here could be extended to the visual detection of a wide range of analytes in the environment by the construction of highly efficient FRET nanoprobes.

Received 8th April 2016,
Accepted 17th June 2016

DOI: 10.1039/c6nr02878k

www.rsc.org/nanoscale

Introduction

The development of new strategies for determination of anions has emerged as a research area of great importance because of the roles of anions in chemical and biological applications.[1–3] As the smallest anion, the fluoride ion plays an important role in human health and environmental processes.[4,5] Appropriate fluoride ingestion will contribute to the prevention of dental caries and promote healthy bone growth. However, excessive fluoride intake may cause fluorosis, urolithiasis and many serious neurodegenerative diseases.[6,7] In order to prevent such problems, the World Health Organization (WHO) recommends monitoring the fluoride levels in local water supplies and stipulates the development of new methods for the quantitative analysis of fluoride.[8] Although conventional analytical techniques for fluoride ion detection including ion chromatography (IC),[9] ^{19}FNMR,[10] fluoride selective electrodes,[11] fluorescence capillary electrophoresis,[12] *etc.* could meet the demand for detection of fluoride ions in water samples, all these methods are either of low sensitivity, poor reproducibility and time-consuming, or require expensive instrumentation and cause additional environmental pollution. Therefore, there is a crucial requirement to develop reliable, fast, easily operated, real-time and on-site techniques to detect fluoride ions in water samples, especially for resource-limited countries and remote regions. The detection strategy has trended toward portable, visual, and easy operation of sensitive techniques such as chemosensors and biosensors. Of various sensing methods, test papers are the most convenient chemo/bio sensors through their visual colorful responses to interesting molecules which can be observed by the naked eye.[13–16]

Because of the high sensitivity, easy operation, and low interference characteristics, fluorescent sensors have been proved to be a powerful tool for rapid and simple analysis of their targets.[17] Compared to the traditional organic fluorophores, such as organic dyes and fluorescent proteins, semiconductor quantum dots (QDs) have attracted extensive research interest as a superior material for fluorescent sensing in the past two decades, due to their unique optical properties, including size-tunable emission, broad absorption spectra,

[a]*School of Chemistry and Chemical Engineering, Hefei University of Technology and Anhui Key Laboratory of Controllable Chemical Reaction & Material Chemical Engineering, Hefei, Anhui 230009, China. E-mail: shmyu@hfut.edu.cn*
[b]*Institute of Intelligent Machines, Chinese Academy of Sciences, Hefei, Anhui 230031, China. E-mail: cljiang@iim.ac.cn*
[c]*Department of Chemistry, University of Science and Technology of China, Hefei, Anhui 230026, China*
[d]*State Key Laboratory of Transducer Technology, Chinese Academy of Sciences, Hefei, Anhui 230031, China*

†Electronic supplementary information (ESI) available. See DOI: 10.1039/c6nr02878k

large effective Stokes shifts and high resistance to photobleaching.[18] However, the toxic components such as heavy metals in QDs might introduce additional pollution into the environment, which consequently limits the wider applications of QD-based sensors. The search for nontoxic alternative QD-like fluorescent nanomaterials has continued for a few years. Carbon-based nanomaterials have recently emerged as the most attractive candidates to produce photoluminescence for the construction of the sensors.[19] As a two-dimensional (2D) nanoscale material, a graphene oxide (GO) nanosheet, prepared by the oxidation of graphite,[20–22] contains not only functional groups of epoxide, phenol hydroxyl, and carboxyl,[23] but also rigid conjugated sp^2 domains/clusters possessing the potential to emit in the visible wavelength range.[24] Furthermore, it bears numerous phenol hydroxyl and epoxy groups at the basal plane and carboxylic groups at the lateral edge, thus providing the direct interaction with biological species and the flexibility of chemical modification. Common GO possesses a finite electronic bandgap and is usually used as a highly efficient fluorescence quencher in many reported chemosensors,[25–27] and it also has very low photoluminescent efficiency because these reactive groups often induce non-radiative recombination of electron–hole pairs.[28–32] However, recent studies suggested that passivation of the epoxy and carboxyl groups could improve the photoluminescence of GO and extend its wider applications in sensors.[33] Meanwhile, GO can enlarge the molecular orientation change and make this effect easier to observe, and also has a high adsorption capacity toward trace analytes. The remarkable properties of GO nanosheets make them very suitable for fluorescent nanoprobes.

Herein, we report a paper sensor based on the photoluminescent GO for the highly sensitive and selective detection of F^- in water, as illustrated in Scheme 1. This design is based on the fluorescence resonance energy transfer (FRET) mechanism between photoluminescent GO and AgNPs through the formation of cyclic esters between phenylborinic acid and 3-amino-1,2-propanediol. The photoluminescent GO nanosheets link with functionalized AgNPs, leading to the quenching of GO fluorescence. In the presence of F^-, the boronate ester is converted to trifluoro borate,[34] which will break the linkage and disassemble photoluminescent GO from AgNPs, resulting in the fluorescence recovery of the quenched photoluminescent GO. This new nanoprobe assembled by a covalent bond allows quantitative analysis of F^- in water with high selectivity and sensitivity. Owing to the huge surface area and a thickness of several nanometers of GO, the ultrathin flexible nanosheets can be easily assembled into the form of paper sheets or directly fabricated on solid substrates which make GO nanosheets an excellent candidate as basic materials for paper chemosensors. On the basis of this characteristic and the fluorescence "off-to-on" mechanism, we further designed a photoluminescent GO paper sensor, which is formed by inkjet-printing GO ink onto a piece of commercial microporous membrane for the ultrasensitive visual detection of F^- in a very simple fashion. This visual paper sensor for the detection of fluoride ions has three unique advantages in fluorescent detection: (1) fluorescent GO is a very suitable sensing substrate for the fabrication of a paper sensor towards water monitoring because of its nontoxicity to the environment, extreme chemical stability and high resistance to photobleaching; (2) the sensing strategy can offer a limit of detection down to the picomole (pM) level; (3) GO paper sensors can render on-site, real-time and visual detection of F^- in water without the aid of large equipment.

Experimental section

Materials

Natural graphite flakes, *N*,*N*-dimethylformamide (DMF), dichlorosulfoxide, tetrahydrofuran (THF), glycine, trisodium

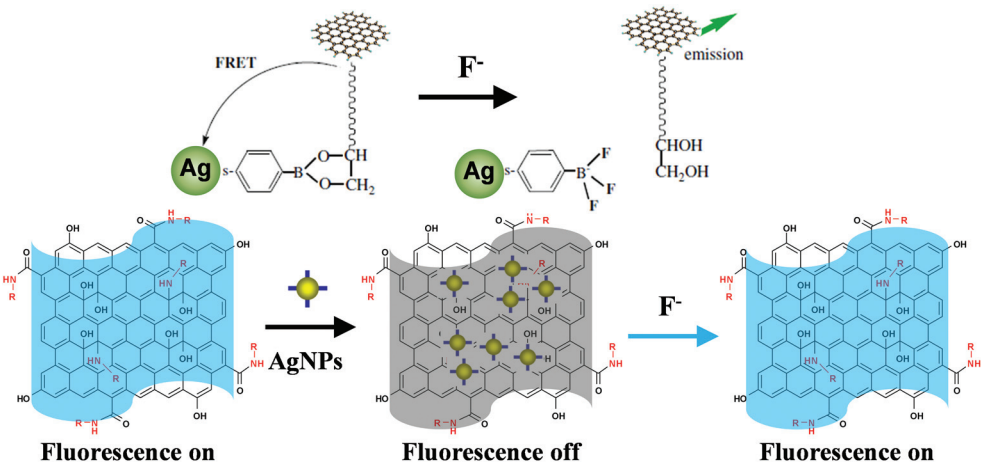

Scheme 1 Fluorescence "off-to-on" mechanism of the GO paper sensor for detection of fluoride ions. The photoluminescent GO nanosheets link with functionalized AgNPs, leading to the quenching of GO fluorescence. The addition of target fluoride ions leads to the disassociation and aggregation of AgNPs, which thus recoveres the fluorescence of GO and facilitates the ultrasensitive detection of fluoride ions.

citrate, silver nitrate (AgN_3) and potassium fluoride (KF) were purchased from Shanghai Chemical Reagent Corporation. 4-Mercaptophenyl-boronic acid, 3-amino-1,2-propanediol, *N*-hydroxysuccinimide (NHS), and *N*-ethyl-*N*′-(3-dimethylaminopropyl)-carbodiimide (EDC) were purchased from Sigma Chemical Corporation. Aqueous solutions were all prepared using ultrapure water (18.2 MΩ cm) from a Millipore water purification system. All chemicals and solvents were obtained from the commercial sources and used directly without further purification, and all glassware was cleaned successively with ultrapure water, and then dried before use.

Synthesis of fluorescence graphene oxide modified by glycine

The initial graphene oxide powder was prepared from natural graphite flakes by a modified Hummers method.[35] The dried graphene oxide (20 mg) was dispersed in 5 mL of *N*,*N*-dimethylformamide, the mixture was then refluxed in dichlorosulfoxide (20 mL) at 80 °C for 24 hours. The supernatant was discarded and the remaining solid was washed twice with anhydrous tetrahydrofuran followed by centrifugation at 10 000 rpm for 10 min. Then, the activated GO acyl chloride (GO–COCl) and glycine (20 mg) were added into anhydrous *N*,*N*-dimethylformamide (2 mL) and mixed at 60 °C for 72 hours. The reaction solution was cooled down to room temperature and dispersed in ethanol (10 mL). A blood red supernatant was obtained after the mixture was vacuum filtered. The GO modified by glycine (GO-glycine) was obtained by drying under high vacuum after rotary evaporation. It was readily redispersed in 10 mM of phosphate buffer saline (PBS) (pH = 7.4) solution to form blood red suspension. The suspension shows bright blue photoluminescence under UV illumination and the maximum photoluminescence intensity at 455 nm under a 360 nm excitation wavelength.

3-Amino-1,2-propanediol conjugation

GO-glycine (10 mg) was dissolved in 10 mL of 10 mM of phosphate buffer saline (PBS) (pH = 7.4) solution. 10 mg of NHS and 20 mg of EDC were added to the GO-glycine solution and incubated for 30 min at room temperature with continuous gentle mixing to activate the carboxylate groups on GO-glycine. After that, 1.50 mg of 3-amino-1,2-propanediol was added to the activated GO-glycine solution. After overnight reaction, the diol-conjugated GO-glycine was separated from the mixture by the dialysis method.

Preparation of mercaptophenyl-boronic acid modified AgNPs (MPBA-AgNPs)

0.01 mg mL^{-1} mercaptophenyl-boronic acid (MPBA) aqueous solution was prepared using ultrapure water. 500 μL of the MPBA aqueous solution were added to 10 mL of the citrate modified AgNP solution under stirring in the dark for 24 h. After that, unbound MPBA was removed by repeated centrifugation (5000 rpm, 20 min), followed by dispersing the precipitation in 10 mL of pure water to obtain MPBA-modified AgNPs.

Fluorescence detection

300 μL of AgNP-MPBA solution was added dropwise into 1 mL of diol-conjugated GO-glycine solution over 30 min to obtain the nanoprobe. 100 μL of 0.10 M PBS (pH = 7.4) buffer solution was added to the probe solutions. Afterwards, different concentrations of F^- were added respectively. The mixture was shaken thoroughly at room temperature prior to fluorescence measurement. After 30 min reaction, the fluorescence spectra were recorded using a 360 nm excitation wavelength. All fluorescence measurements were performed at room temperature under ambient conditions. All the fluorescence intensities were an average of three independent measurements.

Preparation of the paper-based sensor for visual detection of F^-

A common cartridge of a commercial inkjet printer was washed with deionized water until the ink powder was cleared away completely. Then, an aqueous solution of diol-conjugated GO-glycine nanosheets (2 mL, 1.0 mg mL^{-1}) as ink was injected into the vacant cartridge by using a syringe. Subsequently, diol-conjugated GO-glycine can be printed into the words "Fluoride ion" on a piece of polyvinylidene fluoride (PVDF) microporous membrane by an inkjet printer connected to a computer. After the treatment by drying at room temperature, photoluminescent graphene oxide sensors were obtained. Then, the test paper was placed into 10 mL of MPBA-AgNPs for 10 minutes, and these MPBA-AgNPs linked with the diol-conjugated GO-glycine of the words "Fluoride ion". Later, the test paper was taken out, and rinsed with ultrapure water, followed by the evaporation of solution. Owing to the energy transfer between the GO-glycine and AgNPs, these bright blue words on the test paper disappeared under a UV lamp. Subsequently, the test paper was placed into the analyte solutions of F^- for 10 minutes, in the presence of F^-, the boronate ester was converted to trifluoro borate, which caused the breakage of the linkage and disassembled photoluminescent GO from AgNPs. The AgNPs disassociated from these words and aggregated owing to the donor–acceptor interactions mentioned above. Later, the test paper was taken out, and rinsed with ultrapure water, followed by the evaporation of solution. The "Fluoride ion" words gradually appeared with the increase of analyte amounts under a UV lamp.

Analysis of F^- in real tap water and lake water samples

Analysis of F^- in real tap water and lake water samples was performed to evaluate the operating applicability of the nanoprobe in environmental samples. Tap water samples were collected from our lab and the lake water sample was obtained from a local lake. All the water samples collected were first filtered twice using an ordinary qualitative filter paper and 0.45 μm Supor filters to remove the solid suspensions and other impurities. Different concentrations of F^- were added to the as-prepared water samples and then these samples were analyzed using the nanoprobe solutions. The fluorescence spectra were subsequently recorded by using a fluorescence spectrophotometer. The average was obtained from three

independent measurements and presented with a standard deviation. And the samples were also analyzed using the test paper.

Instrumentation

Fluorescence measurement was recorded on a Perkin-Elmer LS-55 luminescence spectrometer (Liantriant, UK). The fluorescence emission spectra were recorded in the wavelength range of 380–650 nm with an excitation wavelength of 360 nm. The slit widths of excitation and emission spectra were both 10 nm. UV-vis absorption was recorded on a Shimadzu UV-2550 spectrometer at room temperature. Infrared spectra of the dried GO, GO-glycine, *etc*. dispersed in KBr pellets were recorded on a Thermo-Fisher Nicolet iS10 FT-IR spectrometer. Photographs were taken with a Canon 350D digital camera.

Results and discussion

The common GO nanosheets were fabricated from the oxidation of graphite by the Hummers method with some modifications. The photoluminescent GO was then prepared according to an effective chemical approach, which consisted of the acylation reaction to form alkylamides and the ring-opening amination of epoxides to yield 1,2-amino alcohols, respectively. The carboxylic groups of GO were first transformed into acyl chlorides, and the acylation and ring-opening reactions were then performed by treatment of GO with glycine, producing the desired GO-glycine, as illustrated in Fig. S1.† Glycine is covalently attached onto the surface of GO, which is evidenced by the FT-IR spectrum (Fig. S2†). A new vibration band around 1720 cm^{-1} of GO-glycine appeared due to the C═O stretching of the primary amide. The peak at 1470 cm^{-1}, corresponding to the stretching vibration of amide (–CONH–), further confirms the amidation reaction. The bands at 1740 cm^{-1} of the carboxylic group still remained after chemical treatment because of the existence of the carboxylic group in glycine. The results suggested the covalent attachment of glycine to the GO surface through the formation of an amide bond. Furthermore, the epoxide band at 1060 cm^{-1} of the original GO completely disappeared in the GO-glycine complex, accompanied by the appearance of a new peak at 1410 cm^{-1} that was assigned to the –C–N– stretching vibration of the amide groups. Meanwhile, the peaks at 1630 cm^{-1} and 1530 cm^{-1} attributed to the stretching vibration of primary amine ($-NH_2$) in glycine could not be noticed in the GO-glycine sample, which implied the exclusion of the physical adsorption of glycine on the surface of GO. It was clearly shown that glycine not only successfully removed the epoxy groups but also covalently attached onto the surface of GO by ring-opening amination of epoxides to yield 1,2-amino alcohols. Moreover, the broad peak at 1625 cm^{-1} owing to the C═C vibration of aromatic rings was observed in both GO samples and GO-glycine, implying that most of the sp^2 characteristic structures in GO-glycine were retained even after the glycine treatment.

The GO-glycine complex exhibits highly blue photoluminescence under UV lamp irradiation which could be obviously observed by the naked eye (Fig. S3†). The fluorescence spectra of GO-glycine showed an emission maximum at 450 nm under an excitation wavelength of 360 nm, and the photoluminescence of GO was enhanced after the functional modification with glycine. Hence, the emission efficiency of the sp^2 domains on GO could be improved by surface passivation which removes reactive sites such as epoxy and carboxylic groups by nucleophilic reactions. Furthermore, the fluorescence enhancement can be evidenced by the change of the absorption spectra of the samples in Fig. S3.† The absorption peak of GO at 230 nm is assigned to the π–π^* transitions of the C═C double bond, and an absorption shoulder of the GO-glycine may be attributed to n–π^* transitions of C═O.

After the glycine treatment, the original absorption band of GO disappeared and a new absorption band appeared at 260 nm, most likely owing to the decrease in the concentration of carboxyl groups within the original GO. Therefore, the above results show that some new photoluminescent groups formed at the surface of GO-glycine, in agreement with the FT-IR spectra of GO-glycine.

It has been proved that it's easy for the formation of cyclic esters between boronic acid and diol in aqueous media owing to their affinity. For the sensing design, 3-amino-1,2-propanediol (diol) is selected to bind carboxyl onto the surface of GO-glycine, using *N*-ethyl-*N*′-(3-dimethylaminopropyl)-carbodiimide (EDC) as a coupling reagent. The formation of GO–diol conjugates can be confirmed by UV-visible absorption spectra and fluorescence spectra. The absorption spectra (Fig. S4†) show a characteristic absorption peak at 260 nm in aqueous solution. After modification by 3-amino-1,2-propanediol, the absorption peak obviously shifts to 266 nm due to the slight increase in the size of GO-glycine. The emission spectrum of the GO-glycine solution (Fig. S5†) demonstrates good symmetry and a narrow spectral width. After conjugation with diol, the fluorescence peak of GO–diol broadens and the maximum emission peak red-shifts slightly, due to the increase of the GO-glycine size.

Fluorescence resonance energy transfer (FRET) from the excited state of the donors to acceptors has been regarded widely as an extremely useful tool for the sensitive determination of molecules.[36–40] As a remarkable fluorescent quencher, AgNPs have been used to detect targets with high sensitivity in FRET systems because of their high extinction coefficients as well as a broad absorption spectrum within the visible light range that overlaps with the emission wavelengths of common energy donors.[41–43] In the current sensing strategy, AgNPs were selected as the fluorescent quencher to construct FRET fluorescence assay. Mercaptophenyl-boronic acid (MPBA) was used to modify AgNPs, which has a higher affinity toward thiols due to the intense Ag–S covalent bond. The resulted MPBA-AgNPs are highly stable in aqueous solution without precipitation for several months at 4 °C. The absorption

spectra of AgNPs (Fig. S6†) have a characteristic surface plasmon resonance absorption peak at 404 nm, and the peak shifts to 410 nm due to the slight increase in the diameter of AgNPs after being modified by MPBA. In addition, the spectrum doesn't exhibit large broadening, indicating good dispersion of AgNPs after the modification. The FTIR spectra (Fig. S7†) of MPBA-modified AgNPs further confirm the strong attachment of thiolated ligands to AgNPs. The characteristic IR absorption peak of the S–H stretching mode (2550–2600 cm^{-1}) of free MPBA molecules disappears in that of MPBA-modified AgNPs, suggesting that the bonding of the ligands to the AgNP surfaces occurs through the –SH end.

The absorption spectrum of MPBA-AgNPs overlaps the fluorescence emission spectrum of GO–diol conjugates (Fig. S8†), which is highly beneficial to the construction of a FRET sensing strategy. Upon addition into the aqueous GO–diol conjugate solution, these MPBA-AgNPs thus link with GO–diol conjugates by the formation of cyclic esters between phenylborinic acid and diol, resulting in GO–diol–MPBA-AgNP nanoprobes that are still highly dispersive in aqueous solution. The formation of cyclic esters between phenylborinic acid and diol was further confirmed by the TEM (Fig. S9†) and the MPBA-AgNPs link onto the surface of GO. Meanwhile, the fluorescence of GO–diol conjugates is strongly quenched by the MPBA-AgNPs through the resonance energy transfer or charge-transfer process, and thus a FRET-based fluorescence sensor was realized. We can simultaneously monitor the gradual quenching of the bright blue fluorescence in the aqueous GO–diol conjugates when increasing the concentrations of MPBA-AgNPs, and the fluorescence completely disappeared under a UV lamp with the concentrations of MPBA-AgNPs up to 0.129 nM. The fluorescence emission intensity of the assay was measured after the addition of various concentrations of MPBA-AgNPs. As can be seen in Fig. 1a, the fluorescence intensity continuously decreased with the increase of MPBA-AgNP concentrations, and the plots of fluorescence quenching efficiencies F/F_0 rapidly decreased with the amount of MPBA-AgNPs in the 1.0 mg mL^{-1} aqueous GO–diol conjugates solution (Fig. 1b). We also treated the GO-glycine solution with un-modified AgNPs, and the results indicated that the strong quenching of the fluorescence of GO–diol conjugates was not due to the inner filter effect (IFE) (Fig. S10†). The dynamics experiments evidenced that the reaction of GO-glycine with MPBA-AgNPs almost completed in ~30 min (Fig. S11†).

Cyclic esters can be easily formed between them in aqueous media because of the affinity of boronic acid and diol, and F^- can break the linkage *via* the formation of fluoride–boron interactions. Therefore, we proposed a "turn-on" fluorescent strategy for the construction of a visual nanoprobe toward F^- detection by just taking the advantage of the unique fluoride–boron interaction. When F^- was added into the GO–diol–MPBA-AgNP probe solutions, the quenched fluorescence was then recovered dramatically due to the formation of a boronate ester bond, which breaks the linkage of cyclic esters and disassembles photoluminescent GO from AgNPs. Boron has an empty p orbit that can easily accept an external lone pair electron, and thus F^- can strongly interact with the boron atom. The center atom boron has an sp^2 hybridized trigonal configuration, and binding of a F^- anion to the center atom boron will generate the corresponding complex with a tetrahedron configuration, which can trigger the sp^2–sp^3 hybridization of boron and weaken the combination between boronic acid and diol.[34] In addition, boronic acids can bind diol moieties with high affinities through reversible boronate formation, and the addition of a F^- anion sets up a second equilibrium between the boronic acid and the diol in the system, which then perturbs the boronic acid–diol equilibrium, resulting in changes in the complex. Consequently, three F^- anions react with the boron atom due to a higher tendency for the fluoride–boron interaction. These structural changes induced disassembling of photoluminescent GO from AgNPs and the fluorescence recovery of the quenched GO–diol conjugates. FTIR spectra were recorded to confirm the mechanism. The characteristic IR absorption peak of the boronate ester bond (1315 cm^{-1}) of GO–diol–MPBA-AgNPs disappears when F^- was added into the quenched GO–diol–MPBA-AgNP solutions (Fig. S12†), suggesting that F^- caused the breakage of the boronate ester bond.

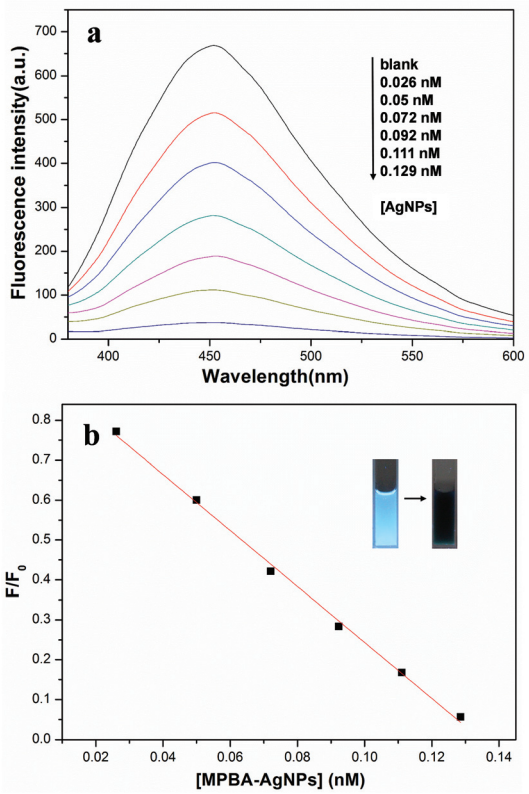

Fig. 1 (a) Fluorescence quenching of the GO-glycine probe solution (1.0 mg mL^{-1}) with the addition of MPBA-AgNPs. (b) Plot of fluorescence quenching as a function of the MPBA-AgNP concentrations. F_0 and F are the fluorescence intensities of the GO-glycine probe solution in the absence and in the presence of MPBA-AgNPs, respectively. The inset photographs show the fluorescence images of the GO-glycine probe solution before (left) and after (right) the addition of MPBA-AgNPs under UV irradiation.

We then validated the above sensory mechanism and its sensitivity for the detection of the fluoride ion. According to the experimental results, the fluorescence of quenched GO–diol–MPBA-AgNP solutions recovered dramatically upon the addition of F^-. Under optimal conditions, the variation of fluorescence intensity in the presence of different concentrations of F^- was recorded, as shown in Fig. 2. There is a low background fluorescence signal before addition of F^- due to the high quenching efficiency of MPBA-AgNPs. The "turn-on" fluorescence enhancement can be easily visualized with the probe solution color changes from dark to blue to bright blue under a 365 nm UV lamp (Fig. 2a), which provides a nice opportunity for detection by the naked eye without the need for elaborate equipment except for a small UV lamp used as an excitation light source. The emission intensity of GO–diol–MPBA-AgNP solutions obviously enhances upon the introduction of F^- (Fig. 2b). As the fluorescence intensity increase is proportional to the F^- concentration, a linear curve of fluorescence intensity *versus* F^- concentration is obtained (Fig. 2c), the linear fitting equation is $y = 24.209 + 807.939x$ ($R^2 = 0.998$), allowing the quantification of F^- in the range of 0.05–0.55 nM. Statistical analysis reveals a limit of detection of F^- as low as 9.07 pM, which was calculated based on 3σ (signal-to-noise ratio) of 10 blank samples.

Meanwhile, the selectivity of detection of F^- was further examined by the addition of other metal ions into the probe solution. Fig. 3 shows the changes in the fluorescence properties of GO–diol–MPBA-AgNPs with the addition of different anions. Of all the anions tested, only the addition of F^- gave a significant recovering response in the fluorescence intensity of the aqueous solution. The addition of other anions did not lead to a measurable fluorescence change. The selectivity observed for F^- over other anions was remarkably high. It can be seen that the relatively high concentrations of Cl^-, Br^-, I^-, HCO_3^-, CH_3COO^-, CO_3^{2-}, HPO_4^{2-}, NO_3^- and SO_4^{2-} (0.55 nM) have little interference on the fluorescence intensity of GO–diol–MPBA-AgNPs. Through experiment, we find that the HS^- could also recover the fluorescence of the probe to a certain extent. However, the interferences of HS^- to the detection of F^- could be effectively avoided by the addition of

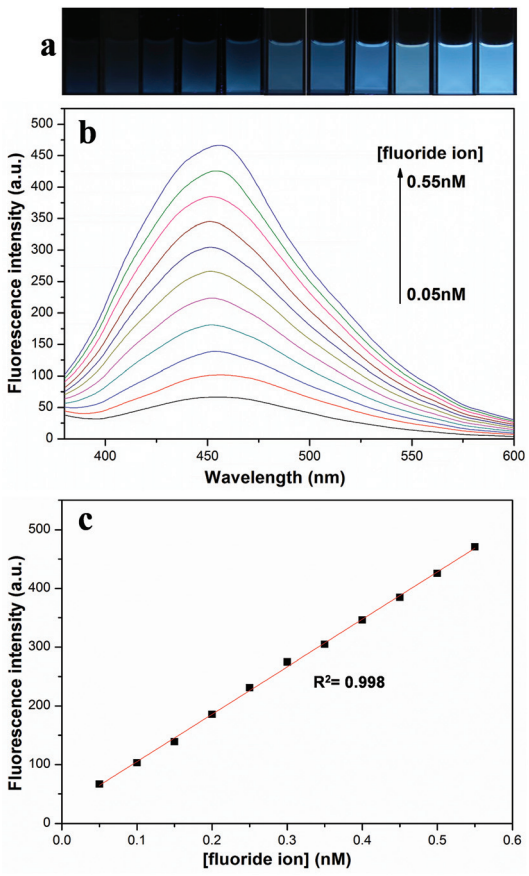

Fig. 2 Fluorescence image set (a) of the GO–diol–MPBA-AgNP solution (1.0 mg mL^{-1}) upon the addition of different amounts of aqueous F^-, the corresponding fluorescence spectra (b) and (c) the plot of fluorescence recovery as a function of the fluoride ion concentrations.

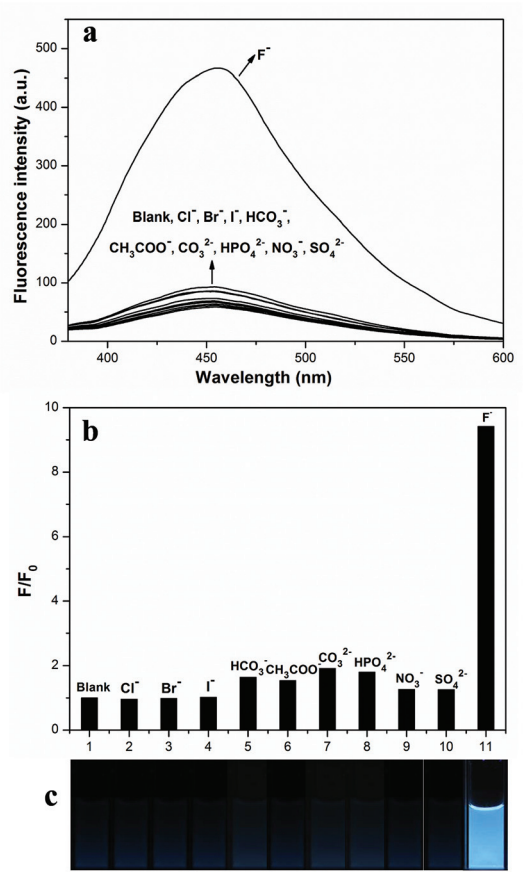

Fig. 3 (a) Fluorescence spectra of the GO–diol–MPBA-AgNP solution in the presence of Cl^-, Br^-, I^-, HCO_3^-, CH_3COO^-, CO_3^{2-}, HPO_4^{2-}, NO_3^- and SO_4^{2-} and F^-, the concentrations of all the anions are 0.55 nM; (b) selectivity of the GO–diol–MPBA-AgNP probe over other anions with the concentration of 0.55 nM, F_0 and F are the fluorescence intensities of the GO–diol–MPBA-AgNP probe solution in the absence and in the presence of an anion, respectively. (c) Fluorescence image set of the GO–diol–MPBA-AgNP solution upon the addition of Cl^-, Br^-, I^-, HCO_3^-, CH_3COO^-, CO_3^{2-}, HPO_4^{2-}, NO_3^- and SO_4^{2-} and F^- (0.55 nM).

N-ethylmaleimide (NEM) as a chelating agent (Fig. S13†). The high selectivity of the present probe towards F^- over other anions can be attributed to the highest Lewis basicity of the F^- ion among all anions and the minimal radius of the F^- ion, further promoting the strong binding of F^- to the boron atom.

To develop a simple, cheap, portable, and reliable paper-based sensor is the ultimate goal for the instant on-site detection in practical applications. Recently, fluorescence nanomaterials have exhibited the potential to prepare paper-based nanosensors for the visual detection of some analytes such as trinitrotoluene and biomolecules. It is well documented that F^- plays an important role in human health and environmental processes. Thus, instant and visual detection of trace F^- in aqueous solution is very crucial for on-site and real-time environmental monitoring. To assess the utility of the visual detection of F^- with the fluorescent GO sensor, a paper-based sensor has been further developed for the visual detection of F^- in aqueous solution. Fluorescent GO-glycine consists of two-dimensional ultrathin nanosheets, and thus provides feasibility for printing the sensors on the paper-like materials. In the case of normal printing papers, the strong background fluorescence under a UV lamp seriously interferes with the colorimetric observations. In particular, the printed GO-glycine nanosheets automatically exfoliate from normal papers or common filter paper upon contacting aqueous solution, which is due to the obvious swelling and dilation of these highly hydrophilic papers. In contrast, the commercial polyvinylidene fluoride (PVDF) microporous membrane has a highly compact and stable structure and a large number of micrometer-scaled (0.22 mm) pores, which do not only overcome the drawbacks of swelling and dilation of normal papers in water, but also significantly increase the fastening of printed GO-glycine nanosheets on this membrane. Meanwhile, the PVDF membrane does not have any intrinsic background fluorescence interference under a UV lamp, which also enhances the fluorescence sensitivity for visual detection.

Aqueous GO–diol conjugate nanosheets (2 mL, 1.0 mg mL^{-1}) acting as a colorless "imaging ink" were first injected into a vacant cartridge of a commercial inkjet printer, as illustrated in the top panel of Fig. 4. The desired word or image is printed onto a piece of PVDF microporous membrane by a common printer connected to a computer. The invisible words "Fluoride ions" can appear in bright blue under a UV lamp, and the edges of the words are very sharp and their fluorescence brightness is completely uniform. Moreover, the brightness of the words could be tunable by the concentration of GO–diol conjugates. These results indicate that the method is highly accurate, reliable, and applicable in the fabrication of sensors on the PVDF membrane. In principle, the printed GO–diol conjugate nanosheets may fold on the surface, creating pockets that could trap MPBA-AgNPs to prevent their dissociation that might reduce the sensitivity of detection. To study the stability of fluorescence of the GO–diol conjugates, the word "Fluoride ions" was printed on the PVDF microporous membrane by an inkjet printer using GO–diol conjugates as the ink, and after drying, the photographs were taken under a UV lamp at an interval of 5 minutes. The images show that the fluorescence is very bright and stable even after immersion in water for more than 30 minutes (Fig. S14†). The experiments indicated that the as-prepared fluorescent GO paper sensors can be utilized for on-site, real-time and visual detection of F^- without the aid of sophisticated equipment.

According to the off-to-on mechanism, F^- was further detected on the test paper. When the test paper printed with GO–diol conjugates was placed into 10 mL of MPBA-AgNPs for 10 minutes, the MPBA-AgNPs linked with the GO–diol conjugates of the words "Fluoride ions". Owing to the energy transfer between the GO–diol conjugates and MPBA-AgNPs, the bright blue words on the test paper disappeared gradually under the illumination of the UV lamp. When the test paper was immersed in the analyte solutions of F^- with different concentrations, the boronate ester was converted to trifluoro borate, which caused the breakage of the linkage and the AgNPs disassociated from the words and aggregated owing to the donor–acceptor interactions. Thus, "Fluoride ions" words gradually appearing with the increase of analyte amounts

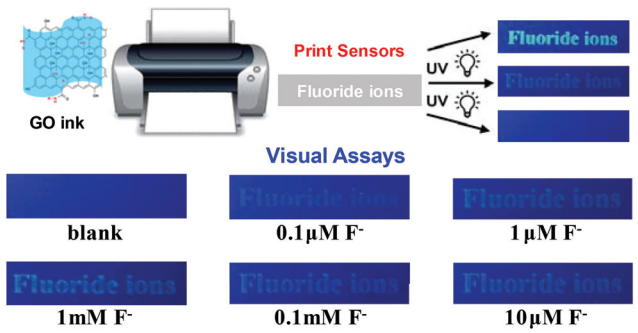

Fig. 4 Visual detection of F^- upon the addition of different concentrations of F^-. All the images were taken under the illumination of a 365 nm UV lamp.

Table 1 Determination of F^- spiked in tap water and real lake water samples using the proposed method

	Tap water			Lake water		
Spiked concentration (nM)	Found (nM)	Recovery (%)	RSD (%)	Found (nM)	Recovery (%)	RSD (%)
0.1	0.103	103.3	2.3	0.107	107.2	2.5
0.3	0.295	98.4	3.6	0.319	106.3	1.7
0.5	0.509	101.9	1.8	0.491	98.2	3.1

shows that the fluorescent GO paper sensors can directly, rapidly, and sensitively detect fluoride ions in aqueous solution, which do not need the complicated amplification reaction and spectroscopic equipment. Thus, the method exhibits the advantages of low cost, easy operation, environmental friendliness and portability.

To further study the practical applicability of the fluorescence method, we investigate samples of local drinking water by spiking different concentrations of F^- to tap water and lake water. As shown in Table 1, excellent recoveries ranging from about 98% to 107% at three different concentrations of F^- (0.1, 0.3, 0.5 nM) were obtained. Furthermore, we spiked F^- of 0.1 μM, 10 μM, and 1 mM into tap water and lake water to validate the visual effect and accuracy of the test paper. As shown in Fig. S15,† "Fluoride ions" words could be visualized under a UV lamp at the concentration of 0.1 μM F^- in tap water and lake water. And at the concentration of 1 mM, the words could be visualized clearly under a UV lamp, which indicates that this method could serve as a practical and convenient method for the detection of F^- in water samples.

Conclusions

In summary, we have reported visual detection of F^- in aqueous solution using a fluorescent GO paper sensor, which is based on a FRET nanoprobe between photoluminescent GO and AgNPs through the formation of cyclic esters between phenylborinic acid and diol. The formed active boronate esters facilitate the efficient FRET. Meanwhile, the F^- anion, a very hard Lewis base, specifically reacts with the boron center and disassembles the AgNP segment, resulting in the fluorescence recovery of the quenched GO–diol conjugates. The excellent selectivity toward F^- was demonstrated in an aqueous solution comparing with other foreign ions, and the developed sensor could detect as low as 9.07 pM F^- in solution. Taking advantage of this phenomenon, a paper-based sensor for the visual detection of aqueous F^- has been successfully developed and the limit of detection of this facile method could reach as low as 0.1 μM as observed by the naked eye. The concept reported herein shows a simple but effective way for aqueous F^- detection and can be extended to the visual detection of a wide range of anions in the environment using this method for the construction of highly efficient FRET nanoprobes.

Acknowledgements

This work was supported by the National Basic Research Program of China (2015CB932002), the China–Singapore Joint Project (2015DFG92510), the Science and Technology Service Network Initiative of Chinese Academy of China (KFJ-SW-STS-172), and the National Natural Science Foundation of China (No. 21371174, 21335006, 21275145, 21277145, 21375131, and 21475135).

References

1 P. A. Gale, *Coord. Chem. Rev.*, 2001, **213**, 79–128.
2 R. Martínez-Máñez and F. Sancenón, *Chem. Rev.*, 2003, **103**, 4419–4476.
3 P. D. Beer and P. A. Gale, *Angew. Chem., Int. Ed.*, 2001, **40**, 486–516.
4 Y. Li, Y. Duan, J. Zheng, J. Li, W. Zhao, S. Yang and R. Yang, *Anal. Chem.*, 2013, **85**, 11456–11463.
5 B. Sui, B. Kim, Y. Zhang, A. Frazer and K. D. Belfield, *ACS Appl. Mater. Interfaces*, 2013, **5**, 2920–2923.
6 S. Y. Kim, J. Park, M. Koh, S. B. Park and J. I. Hong, *Chem. Commun.*, 2009, 4735–4737, DOI: 10.1039/b908745a.
7 B. Ke, W. Chen, N. Ni, Y. Cheng, C. Dai, H. Dinh and B. Wang, *Chem. Commun.*, 2013, **49**, 2494–2496.
8 J. Fawell, K. Bailey, J. Chilton, E. Dahi, L. Fewtrell and Y. Magara, *World Health Organization (WHO) 2006*, IWA Publishing, 2006.
9 H. Yiping and W. Caiyun, *Anal. Chim. Acta*, 2010, **661**, 161–166.
10 D. A. P. Tanaka, S. Kerketta, M. A. L. Tanco, T. Yokoyama and T. M. Suzuki, *Sep. Sci. Technol.*, 2002, **37**, 877–894.
11 R. A. Rocha, D. Rojas, M. J. Clemente, A. Ruiz, V. Devesa and D. Velez, *J. Agric. Food Chem.*, 2013, **61**, 10708–10713.
12 I. C. Guimarães, C. C. Rezende, J. A. F. da Silva and D. P. de Jesus, *Talanta*, 2009, **78**, 1436–1439.
13 Q. Mei and Z. Zhang, *Angew. Chem., Int. Ed. Engl.*, 2012, **51**, 5602–5606.
14 K. Zhang, H. Zhou, Q. Mei, S. Wang, G. Guan, R. Liu, J. Zhang and Z. Zhang, *J. Am. Chem. Soc.*, 2011, **133**, 8424–8427.
15 K. Zhang, T. Yu, F. Liu, M. Sun, H. Yu, B. Liu, Z. Zhang, H. Jiang and S. Wang, *Anal. Chem.*, 2014, **86**, 11727–11733.
16 C. Yuan, B. Liu, F. Liu, M. Y. Han and Z. Zhang, *Anal. Chem.*, 2014, **86**, 1123–1130.
17 X. Zhao, S. Li, L. Xu, W. Ma, X. Wu, H. Kuang, L. Wang and C. Xu, *Biosens. Bioelectron.*, 2015, **70**, 372–375.
18 D. M. Guldi, B. M. Illescas, C. M. Atienza, M. Wielopolski and N. Martin, *Chem. Soc. Rev.*, 2009, **38**, 1587–1597.
19 Q. Mei, K. Zhang, G. Guan, B. Liu, S. Wang and Z. Zhang, *Chem. Commun.*, 2010, **46**, 7319–7321.
20 R. Pasricha, S. Gupta and A. K. Srivastava, *Small*, 2009, **5**, 2253–2259.
21 D. Yu and L. Dai, *J. Phys. Chem. Lett.*, 2010, **1**, 467–470.
22 D. R. Dreyer, S. Park, C. W. Bielawski and R. S. Ruoff, *Chem. Soc. Rev.*, 2010, **39**, 228–240.
23 F. Li, Y. Huang, Q. Yang, Z. Zhong, D. Li, L. Wang, S. Song and C. Fan, *Nanoscale*, 2010, **2**, 1021–1026.
24 X. Sun, Z. Liu, K. Welsher, J. Robinson, A. Goodwin, S. Zaric and H. Dai, *Nano Res.*, 2008, **1**, 203–212.
25 C.-H. Lu, H.-H. Yang, C.-L. Zhu, X. Chen and G.-N. Chen, *Angew. Chem., Int. Ed.*, 2009, **48**, 4785–4787.
26 J. Balapanuru, J.-X. Yang, S. Xiao, Q. Bao, M. Jahan, L. Polavarapu, J. Wei, Q.-H. Xu and K. P. Loh, *Angew. Chem.*, 2010, **122**, 6699–6703.

27 Y. Zhu, Y. Cai, L. Xu, L. Zheng, L. Wang, B. Qi and C. Xu, *ACS Appl. Mater. Interfaces*, 2015, **7**, 7492–7496.
28 J. E. Riggs, Z. Guo, D. L. Carroll and Y.-P. Sun, *J. Am. Chem. Soc.*, 2000, **122**, 5879–5880.
29 S.-J. Yu, M.-W. Kang, H.-C. Chang, K.-M. Chen and Y.-C. Yu, *J. Am. Chem. Soc.*, 2005, **127**, 17604–17605.
30 Y.-P. Sun, B. Zhou, Y. Lin, W. Wang, K. A. S. Fernando, P. Pathak, M. J. Meziani, B. A. Harruff, X. Wang, H. Wang, P. G. Luo, H. Yang, M. E. Kose, B. Chen, L. M. Veca and S.-Y. Xie, *J. Am. Chem. Soc.*, 2006, **128**, 7756–7757.
31 H. Zhu, Y. Zhang, L. Zhang, T. Yu, K. Zhang, H. Jiang, L. Wu and S. Wang, *J. Mater. Chem. C*, 2014, **2**, 7126.
32 V. N. Mochalin and Y. Gogotsi, *J. Am. Chem. Soc.*, 2009, **131**, 4594–4595.
33 Z. Houjuan, Z. Wen, Z. Kui and W. Suhua, *Nanotechnology*, 2012, **23**, 315502.
34 M. Xue, X. Wang, L. Duan, W. Gao, L. Ji and B. Tang, *Biosens. Bioelectron.*, 2012, **36**, 168–173.
35 G. Jiang, A. S. Susha, A. A. Lutich, F. D. Stefani, J. Feldmann and A. L. Rogach, *ACS Nano*, 2009, **3**, 4127–4131.
36 W. S. Hummers and R. E. Offeman, *J. Am. Chem. Soc.*, 1958, **80**, 1339–1339.
37 J. F. Lovell, M. W. Chan, Q. Qi, J. Chen and G. Zheng, *J. Am. Chem. Soc.*, 2011, **133**, 18580–18582.
38 Y. Xie, A. V. Dix and Y. Tor, *J. Am. Chem. Soc.*, 2009, **131**, 17605–17614.
39 M. H. Lee, D. T. Quang, H. S. Jung, J. Yoon, C.-H. Lee and J. S. Kim, *J. Org. Chem.*, 2007, **72**, 4242–4245.
40 J. Hu, G. Zhang, Y. Geng and S. Liu, *Macromolecules*, 2011, **44**, 8207–8214.
41 M. Lessard-Viger, M. Rioux, L. Rainville and D. Boudreau, *Nano Lett.*, 2009, **9**, 3066–3071.
42 J. Zhang, Y. Fu and J. R. Lakowicz, *J. Phys. Chem. C*, 2007, **111**, 50–56.
43 K.-S. Kim, J.-H. Kim, H. Kim, F. Laquai, E. Arifin, J.-K. Lee, S. I. Yoo and B.-H. Sohn, *ACS Nano*, 2012, **6**, 5051–5059.